Inhibition of brain tumor growth by intravenous poly (β-L-malic acid) nanobioconjugate with pH-dependent drug release

Hui Ding[a], Satoshi Inoue[a], Alexander V. Ljubimov[b,c], Rameshwar Patil[a], Jose Portilla-Arias[a], Jinwei Hu[a], Bindu Konda[a], Kolja A. Wawrowsky[d], Manabu Fujita[b], Natalya Karabalin[a], Takako Sasaki[e], Keith L. Black[a], Eggehard Holler[a,f,1], and Julia Y. Ljubimova[a,c,1]

Departments of [a]Neurosurgery, [b]Surgery, [c]Biomedical Sciences, and [d]Academic Affairs, Cedars-Sinai Medical Center, Los Angeles, CA 90048; [e]Department of Experimental Medicine I, Nikolaus-Fiebiger Center of Molecular Medicine, University of Erlangen-Nürnberg, D-91954 Erlangen, Germany; and [f]Institut für Biophysik und Physikalische Biochemie der Universität Regensburg, D-93053 Regensburg, Germany

Edited by Alexander M. Klibanov, Massachusetts Institute of Technology, Cambridge, MA, and approved August 27, 2010 (received for review March 25, 2010)

Effective treatment of brain neurological disorders such as Alzheimer's disease, multiple sclerosis, or tumors should be possible with drug delivery through blood–brain barrier (BBB) or blood–brain tumor barrier (BTB) and targeting specific types of brain cells with drug release into the cell cytoplasm. A polymeric nanobioconjugate drug based on biodegradable, nontoxic, and nonimmunogenic polymalic acid as a universal delivery nanoplatform was used for design and synthesis of nanomedicine drug for i.v. treatment of brain tumors. The polymeric drug passes through the BTB and tumor cell membrane using tandem monoclonal antibodies targeting the BTB and tumor cells. The next step for polymeric drug action was inhibition of tumor angiogenesis by specifically blocking the synthesis of a tumor neovascular trimer protein, laminin-411, by attached antisense oligonucleotides (AONs). The AONs were released into the target cell cytoplasm via pH-activated trileucine, an endosomal escape moiety. Drug delivery to the brain tumor and the release mechanism were both studied for this nanobiopolymer. Introduction of a trileucine endosome escape unit resulted in significantly increased AON delivery to tumor cells, inhibition of laminin-411 synthesis in vitro and in vivo, specific accumulation in brain tumors, and suppression of intracranial glioma growth compared with pH-independent leucine ester. The availability of a systemically active polymeric drug delivery system that passes through the BTB, targets tumor cells, and inhibits glioma growth gives hope for a successful strategy of glioma treatment. This delivery system with drug release into the brain-specific cell type could be useful for treatment of various brain pathologies.

glioma treatment | polymalic acid | laminin-411 | endosomal escape | blood–brain barrier

Brain gliomas are among the most aggressive and lethal cancers. At present, efficient drugs for treatment of gliomas are very limited (1). A hallmark of current cancer treatment is inhibition of tumor angiogenesis (2, 3). Antiangiogenic inhibitors of VEGF receptors and VEGF-independent inhibitors combined with chemotherapy have shown some promise, but the patients' survival in clinical trials was not significantly changed (4). We documented overexpression of tumor-specific vascular basement membrane protein laminin-411 in glioblastoma and its association with tumor recurrence and decreased patients' survival time (5, 6). Laminin-411 consists of three different polypeptide chains, and it was hitherto impossible to efficiently block its synthesis in vivo by existing technologies. In our nanoconjugate, two antisense oligonucleotides (AONs) against laminin α4 and β1 chains were covalently attached and delivered through the blood–brain tumor barrier (BTB). Although the microvascular BTB is more permissible than the blood–brain barrier (BBB), it still retains BBB characteristics (7, 8), hampering drug delivery to brain tumors. Antibodies to certain cell surface proteins, including transferrin receptor (TfR), can pass the BBB and BTB by endothelial transcytosis and then direct carrier systems with attached drugs into tumor cells by receptor-mediated endocytosis (9–13).

Polymer conjugates introduce other possibilities to treat cancers by targeting specific tumor markers and providing precise inhibitor delivery to the tumor with minimum side effects (3, 14, 15). The endocytosed carriers, including polymers, are routed to the endosomal pathway, and their design must ensure the drug escape from the endosomes into the cytoplasm to avoid lysosomal degradation. Cytoplasmic delivery using cell penetrating peptides (CPPs) acting directly on cell membranes is a possible mechanism for drug trafficking across the plasma membrane (16), but CPPs are not specific to the cell type. Receptor-targeted cytoplasmic delivery through endosome disruption is a safe and efficient approach avoiding potentially cytotoxic permeation through the plasma membrane. It can be achieved by a pH-sensitive endosome-specific, membrane-disrupting moiety that takes advantage of the low pH (5.0–6.5) in the endosome/lysosome compartments.

Several pH-dependent escape devices were designed, such as polyethyleneimine (PEI), which is protonated during endosome acidification (17). These polymers, however, are of limited use due to their cytotoxicity (18). Instead, nontoxic lysogenic peptides, such as Glu-Ala-Leu-Ala (GALA) (19, 20) derived from certain viruses or bacteria, are used for endosome escape of micelles and liposomes (21) or are covalently bound to nanoconjugates to deliver water-soluble proteins, antibodies, and nucleic acids (9, 22).

The nanoconjugate based on poly(β-L-malic acid) (PMLA) that is introduced here meets all criteria for nanomedicine drugs (23) and is a promising candidate for future clinical use, alone or in combination with other treatments for brain cancer. This nanopolymeric drug is designed for i.v. brain tumor treatment using a targeted pH-dependent endosome escape unit. A similar delivery system might be used to treat other brain pathological conditions.

Results

Synthesis of Polymalic Acid-Based Nanoconjugates. Nanoconjugates of varying composition were synthesized. A schematic of a conjugate with all functional groups is shown in Fig. 1*A*, and a simplified chemical formula in the Fig. S1. NHS-activated carboxylates of polymalic acid were first conjugated with H_2N-Leu-Leu-Leu-OH (LLL), H_2N-Leu-Leu-Leu-NH_2, H_2N-Leu-ethylester (LOEt), 2-

Author contributions: H.D., A.V.L., M.F., K.L.B., E.H., and J.Y.L. designed research; H.D., S.I., R.P., J.P.-A., J.H., B.K., K.A.W., M.F., N.K., and J.Y.L. performed research; T.S. contributed new reagents/analytic tools; H.D., S.I., A.V.L., J.P.-A., T.S., K.L.B., E.H., and J.Y.L. analyzed data; and H.D., A.V.L., E.H., and J.Y.L. wrote the paper.

The authors declare no conflict of interest.

This article is a PNAS Direct Submission.

[1]To whom correspondence may be addressed. E-mail: hollere@cshs.org or ljubimovaj@cshs.org.

This article contains supporting information online at www.pnas.org/lookup/suppl/doi:10.1073/pnas.1003919107/-/DCSupplemental.

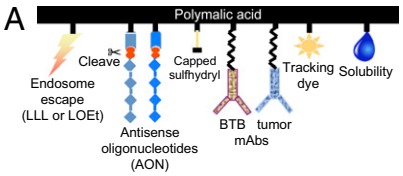

B

Nanoconjugate	MW* (kDa)	Endosome escape (%) LLL	Endosome escape (%) LOEt	AON (%)	Capped -SH (%)	Anti-TfR mAb (%) Mouse	Anti-TfR mAb (%) Human	-COOH (%)
P/LLL	220	40						60
P/LOEt	153		40					60
P/LLL/AON/IgG	728	40		2.5	2.25	0.25**		55
P/LOEt/AON/IgG	661		40	2.5	2.25	0.25**		55
P/LLL/AON/Hu/Ms	1051	40		2.5	2	0.25	0.25	55
P/LOEt/AON/Hu/Ms	984		40	2.5	2	0.25	0.25	55
P/LLL/AON/ Hu	728	40		2.5	2.25		0.25	55
P/LOEt/AON/Hu	661		40	2.5	2.25		0.25	55
P/AON/Hu	608			2.5	2.25		0.25	95

*Molecular weight calculated on the basis of Mn 100,000 for polymalic acid
**(%) denotes the percent fraction of polymer carboxylates conjugated
***mAb was substituted by human nontargeting IgG

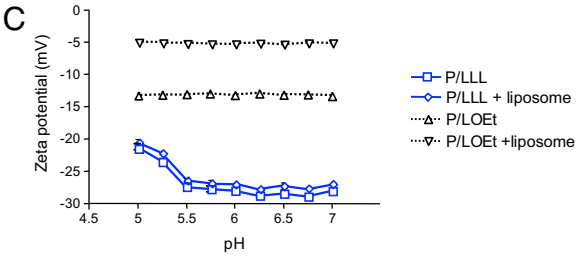

Fig. 1. Nanoconjugates with polymalic acid platform and their ζ potentials. (*A*) Cartoon of PMLA-based nanoconjugate. (*Left* to *Right*) endosome escape unit (LLL or LOEt), AONs to laminin-411 α4 and β1 chains, disulfide linkages cleaved by cytoplasmic glutathione, capped unused sulfhydryl, mAb (Ms) targeting BTB endothelium (mouse TfR), mAb (Hu) targeting tumor cells (human TfR), tracking dye Alexa Fluor 680, pendant carboxylates for water solubility. (*B*) Table listing nanoconjugates and their molecular weight and composition. (*C*) ζ potential for P/LLL and P/LOEt at variable pH. ζ potential in the absence or presence of liposomes was measured under conditions when membrane disruption and leakage had been completed within 5–10 min. P/LOEt potential was significantly shifted in the presence of liposomes but only a marginal shift was seen for P/LLL. This indicated that most P/LOEt was on the liposomes, but most P/LLL was in the free solute state. Measurements were performed with 200 μg/mL P/LLL or P/LOEt and in the presence of 160 μM lipid (liposomes).

mercapto-1-ethylamine. The newly introduced sulfhydryl groups were converted to disulfides with thiolated morpholino AON and to thioethers with maleimidated mAbs and optionally with maleimidated fluorophore Alexa Fluor 680. The composition of synthesized nanoconjugate and pendant group functions are shown in Fig. 1*B*. The composition was confirmed by analytical tests to completely correspond to the synthetic strategy. The calculated molecular weight values compared within 15% with experimental absolute molecular weights by light scattering, which also confirmed the absence of particle aggregation. Sizes by dynamic light scattering ranged from 6.6 nm for PMLA to 18 ± 2 nm for P/LLL/AON/Hu/Ms and 22 ± 2 nm for P/LOEt/AON/Hu/Ms. The ζ potentials (pH 7.0) ranged from −27 ± 1 mV for polymalic acid, −9.4 ± 0.7 mV for P/LLL/AON/Hu/Ms to −5.2 ± 0.4 mV for P/LOEt/AON/Hu/Ms; the potentials of LLL containing conjugates was pH-dependent (Fig. 1*C*). The half-life of the lead nanoconjugate P/LLL/AON/Hu/Ms was 24 h at 37 °C in PBS and similarly in human plasma.

pH-Dependent Membrane Disruption for Nanoconjugate Escape from Endosomes. The TfR-targeting nanoconjugates were released from endosomes/lysosomes through constitutive or pH 5.0–5.5 activated membrane disruption. Two versions of membrane disruption units were used: pH-dependent P/LLL (PMLA conjugated with 40% LLL) and pH-independent P/LOEt (PMLA conjugated with 40% LOEt) (24, 25). At pH 5 both nanoconjugates were membrane disruptive, with similar concentration dependence (Fig. 2*A*). When AONs and mAbs were added to P/LLL/AON/IgG and P/LOEt/AON/IgG nanoconjugates, the leakage remained high (80–90%) (Fig. 2*B*), indicating that membrane disruption activity survived conjugation of AONs and mAb. At physiological pH 7.4, P/LLL conjugates were inactive, whereas membrane disruption by P/LOEt conjugates remained (Fig. 2*C*). P/LOEt activity was high over the investigated pH range, but P/LLL activity was only high at pH 5–5.5 and abruptly dropped at pH 6 (Fig. 2*D*). The pH dependence mirrored the range of acidification in late endosomes/lysosomes. This justified using P/LLL conjugates for endosome-specific escape. In contrast to P/LOEt conjugates, the specific acidification requirement for P/LLL conjugates would not allow cell membrane disruption at neutral pH.

Leucine and its derivatives may form strong hydrophobic interactions allowing assembly into hydrophobic patches and/or can insert directly into lipid membrane bilayers and provoke their disruption (26, 27). This may be the mechanism of membrane interaction with studied nanopolymers. However, LLL carries a charged terminal carboxylate that cannot be accommodated into a lipohilic environment unless carboxylate is neutralized by protonation. By acid–base P/LLL titration, this protonation followed a pK_a 5.5, and this pH dependence paralleled the leakage dependence in Fig. 2*D*. P/LOEt did not contain this ionizable group and did not show pH dependence. When LLL was replaced by LLL–NH_2 with a non-ionizable terminal amide group instead of carboxylate, pH dependence and liposome leakage became similar to LOEt.

The simplest reaction mechanism implies that polymer and liposome bind before the lysis occurs. The concentration dependence in Fig. 2 *A*–*C* may indicate similar binding affinities for P/LLL and P/LOEt to the liposome membrane at pH 5.0 and a very low affinity for P/LLL at pH 7.4 due to the carboxylate charge. P/LOEt and P/LLL liposome membrane affinities dramatically diverged as indicated by confocal microscopy (Fig. 2*E*) and ζ potential (Fig. 1*C*). P/LOEt readily bound to the liposome membrane at neutral pH 7.4, but P/LLL amounts were too low to be detected (Fig. 2*E*). The ζ potential of P/LOEt did not change as a function of pH either in the presence or absence of liposome (Fig. 1*C*). The liposome ζ potential is near zero, and its contribution is negligible. In the presence of liposome, ζ potential of P/LOEt increased from −13 to −5. This change accounts for various parameters that affect the electrophoresis underlying ζ potential measurement and may indicate that the majority of P/LOEt was sticking to the liposome after membrane disruption and leakage. Minor amounts of free P/LOEt would not be detectable by this technique. In contrast, P/LLL ζ potential is pH-dependent (Fig. 1*C*), the pH sensitivity correlating well with pH-dependent liposome leakage activity. The inefficiency of P/LLL in staining liposomes could indicate that small amounts of P/LLL bound to the liposome were below the Zetasizer detection limit.

Overall, nanoconjugates with LOEt readily bound to lipid membranes and in addition to their disruption gave rise to side effects at physiological pH that were not seen with LLL conjugates. This "stickiness" at physiological pH could induce cell toxicity and also systemic depletion of the circulating nanoconjugate after i.v. injection, reducing its availability at the tumor site.

Cell Viability and Increased Suppression of Target Laminin-411 Synthesis with pH-Dependent Endosome Escape Unit. Using P/LLL- and P/LOEt-containing nanoconjugates, cell viability was tested on the human glioma cell line U87MG. P/LLL was nontoxic at all concentrations (≤2 mg/mL), but P/LOEt decreased cell viability at

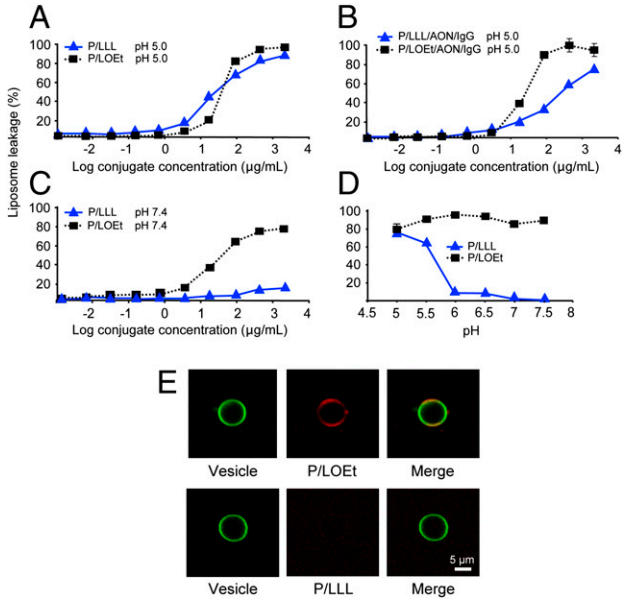

Fig. 2. Membrane disruption activity of P/LLL and P/LOEt and their binding to liposomes. (*A*) Concentration dependence of P/LLL and P/LOEt membrane disruption activity at pH 5.0 measured by the liposome leakage assay. The degree of leakage refers to complete leakage in the presence of 0.25% (vol/vol) Triton-X 100. (*B*) Membrane disruption activity for nanoconjugates P/LLL/AON/IgG and P/LOEt/AON/IgG at pH 5. It is not abolished over the range of concentrations by the conjugation of AON and antibody. (*C*) Retention of membrane-disrupting activity at pH 7.4 by P/LOEt and its loss by P/LLL. (*D*) Membrane disruption for P/LLL and P/LOEt (each 50 μg/mL) as a function of pH. Only P/LLL membrane disruption activity is pH-dependent following an apparent pK_a 5.5. (*E*) Binding of P/LOEt and P/LLL to liposomes at neutral pH. Confocal microscopy showing colocalization of P/LOEt and giant artificial liposomes. P/LLL and P/LOEt were conjugated with rhodamine (red). Giant liposomes were labeled with NBD [N(1)-(7-nitrobenzo[c][1,2,5]oxadiazol-4-yl)propane-1,3-diamine] (green). (*Upper*) Large amounts of P/LOEt stuck to the vesicle membrane; liposomes and P/LOEt colocalized at pH 7.4 (yellow). (*Lower*) Binding of rhodamine-labeled P/LLL to liposomes could not be detected. Concentrations of conjugates were 20 μg/mL. The data correlate well with ζ potential measurement (Fig. 1*C*).

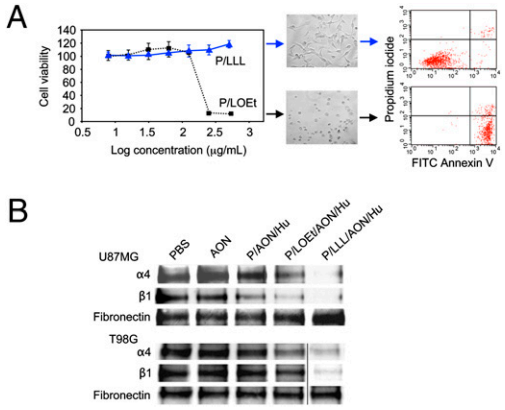

Fig. 3. Human U87MG and T98G glioma cell treatment in vitro with nanoconjugates containing pH-dependent or pH-independent endosome escape units. (*A*) Effects of LLL and LOEt endosomal escape units on U87MG cell viability. Arrows relate to microscopic views (20× magnification) after 24 h treatment with 0.5 mg of either nanoconjugate. The cells treated with P/LOEt unlike P/LLL had low viability at high concentrations (*Left*) and were in early apoptosis (*Center*). (*Right*) Representative FACS analysis of cell death after double staining of cells with propidium iodide and FITC Annexin V. Note markedly increased fraction of apoptotic cells after treatment of cells with P/LOEt as compared with P/LLL. (*B*) Inhibition of laminin-411 α4 and β1 chain synthesis in human U87MG and T98G glioma cells after treatment with PBS, AON, P/AON/Hu (lacking endosomal escape unit), P/LOEt/AON/Hu, and P/LLL/AON/Hu (1.4 μM with regard to AON). Samples were prepared from the culture supernatant at the end of the treatment and subjected to Western blot analysis. P/LLL/AON/Hu was the most effective in inhibiting the synthesis of both laminin-411 α4 and β1 chains. Secreted fibronectin was used to normalize gel loading.

as low as 0.15 mg/mL (Fig. 3*A*, *Left*). At 0.5 mg/mL P/LOEt, cells shrunk and rounded up within 2 h, whereas no such changes were seen with P/LLL (Fig. 3*A*, *Center*). Similar data were obtained with human T98G and rat RG62 gliomas and human breast cancer MDA MB-231 cells. By FACS analysis, the shrunk and rounded cells were mainly in early apoptosis phase (annexin V-positive) (Fig. 3*A*, *Right*), although some increase in necrosis [propidium iodide (PI)-positive] (Fig. 3*A*, *Right*) was also evident.

Western blot analysis of conditioned media confirmed that AONs were efficiently delivered by P/LLL/AON/Hu and P/LOEt/AON/Hu into the cytoplasm of U87MG and T98G glioma cells and that they inhibited the synthesis of laminin-411 α4 and β1 chains (Fig. 3*B*). In the absence of endosomal escape (in the nanoconjugate P/AON/Hu), the synthesis was markedly less affected. Free AONs that could not penetrate cell membranes showed no inhibition (Fig. 3*B*). The data confirmed nanoconjugate functional activities, including TfR binding and internalization, endosomal uptake and escape, and inhibition of laminin-411 synthesis. Nanoconjugates with LLL or LOEt were both active; however, P/LLL/AON/Hu with pH-dependent endosomal escape unit was more potent (Fig. 3*B*).

Colocalization of the Polymer Platform and Antisense Oligonucleotides in Cytoplasm. To confirm that the polymer platform and AONs entered the endosomal pathway together in U87MG and T98G glioma cells, the nanoconjugate P/LLL/AON/Hu was double-labeled with Lissamine at AON and Alexa Fluor 680 at PMLA. By confocal microscopy (Fig. S2), the PMLA platform (green) and AONs (red) colocalized (yellow) in intracellular entities, which coincided (white) with stained endosomal membranes (blue) (Fig. S2*A*). The number of green and red vesicles decreased over time during a 3-h incubation period (Fig. S2*B*). The decrease coincided with diffuse staining around these entities, in agreement with induced leakage by membrane disruption. Statistical analysis of colocalization expressed as Pearson's correlation coefficients (28) (Fig. S2*C*) indicated significant colocalization of PMLA and AON and of each of them with endosomes at 0 h. However, at 3 h, endosomal marker and nanoconjugate colocalization decreased.

Imaging Analysis of Drug Distribution and Accumulation in Tumor and Normal Brain Tissues in Vivo. For these experiments, two mAbs were attached to the PMLA platform. Anti-mouse TfR mAb was used for transporting drugs through the mouse endothelial host system, and anti-human TfR mAb served for targeting implanted human tumor cells. Imaging analysis 24 h after i.v. injection showed that nanoconjugate with anti-mouse TfR mAb delivered only a low amount of drug into the intracranial human U87MG tumor (Fig. 4*A*, *Upper Left*). With anti-human TfR mAb attached to nanoconjugate, drug accumulation in the tumor increased (Fig. 4*A*, *Upper Center*). These data are consistent with the facilitation of polymer passage through BTB by the enhanced permeability and retention (EPR) effect. In the presence of both endothelium- and tumor-targeting mAbs (anti-mouse and anti-human TfR, respectively), P/LLL/AON/Hu/Ms drug predictably showed the highest accumulation of all variants (Fig. 4*A*, *Upper Right*).

We next compared brain tumor-specific accumulation of polymeric drugs containing LLL or LOEt endosomal escape units. In both cases, the drug accumulation 24 h after i.v. injection persisted mainly in brain tumor and to some extent in drug-clearing organs, livers and kidneys. The drug was no longer detected after 72 h. In

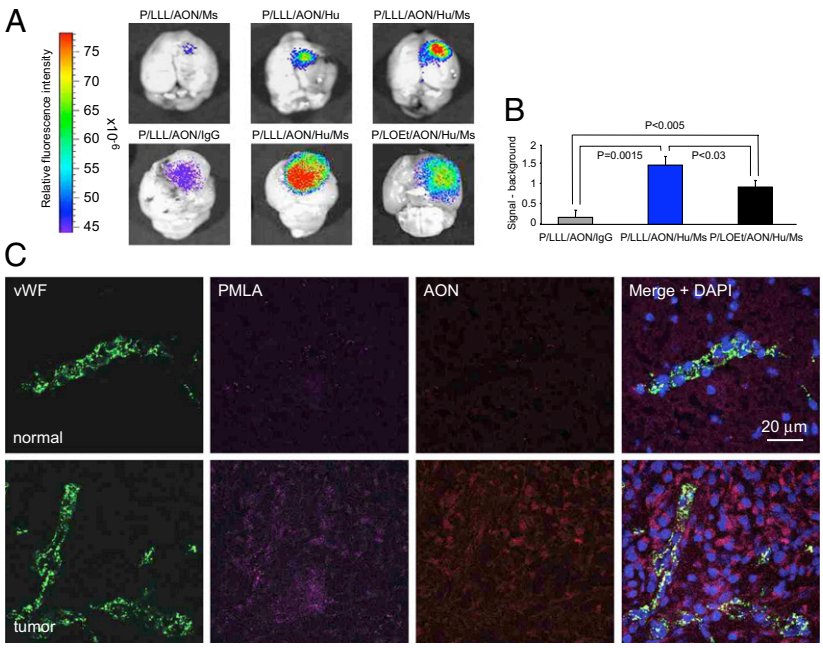

Fig. 4. Imaging analysis of U87MG human brain tumor implanted in mice 24 h after i.v. injection of nanoconjugate variants. Tumor cells (10^5) were implanted intracranially and animals were treated with nanoconjugates after 21 d. Brains were isolated and PBS perfused. The nanoconjugates were P/LLL/AON/Ms (Ms = anti-mouse TfR), P/LLL/AON/Hu (Hu = anti-human TfR), P/LLL/AON/Hu/Ms, P/LOEt/AON/Hu/Ms, and P/LLL/AON/IgG (unrelated IgG). Representative results are shown. (*A*, *Upper*) Alexa Fluor 680-labeled nanoconjugates with Ms, Hu, and Ms/Hu were injected i.v. Different experiments are shown in *Upper* and *Lower*. (*Upper*) the nanoconjugate with both Ms and Hu mAbs showed the highest tumor accumulation. P/LLL/AON/Hu accumulated markedly better than P/LLL/AON/Ms, although Hu in contrast to Ms would not support transcytosis through mouse endothelium. This effect was ascribed to efficient drug withdrawal into the tumor cells after low-level EPR-mediated delivery into the tumor interstitium. The withdrawal effect could account for high accumulation. (*Lower*) LLL presence ensured higher drug tumor accumulation than LOEt, whereas a control nanoconjugate with unrelated IgG showed low accumulation (Xenogen IVIS 200 imaging). (*B*) Drug accumulation in *A, Lower*, representing the signal with subtracted background was quantitated by $(F - F_o)/F_o$. Averaged intensities F and F_o refer to equally sized areas of the tumor and the reference nontumor area, respectively. Means ± SD of three independent measurements are shown. There is significantly higher accumulation of P/LLL/AON/Hu/Ms than of P/LOEt/AON/Hu/Ms in the tumor tissue ($P < 0.03$). (*C*) Confocal microscopy of brain cryostat sections after i.v. injection of double-labeled P/LLL/AON/Hu/Ms nanoconjugate in vivo. The PMLA platform was labeled with Alexa Fluor 680 (magenta) and the AONs with Lissamine (red). Vessels were revealed by immunostaining for vWF (green). (*Upper*) There is little signal of PMLA and AON in the normal brain tissue contralateral to the tumor. (*Lower*) Both PMLA and AON show distinct accumulation in the tumor tissue. They display significant colocalization in the tumor cell cytoplasm (purple, *Right*).

24 h, drug-tumor accumulation of P/LLL/AON/Hu/Ms (Fig. 4*A*, *Upper Right*) was 1.5 times higher ($P < 0.03$) than that of P/LOEt/AON/Hu/Ms variant (Figs. 4*A*, *Lower Center*, and *B*). Because both nanoconjugates use exactly the same targeting strategy, their difference in tumor accumulation could be due to their differences in membrane disrupting units LLL or LOEt, which corresponds well to data shown on Fig. 2. Control P/LLL carrying a nontargeting IgG (P/LLL/AON/IgG) accumulated in the tumor 90% less than P/LLL/AON/Hu/Ms with two targeting antibodies ($P = 0.0015$) (Fig. 4*A*, *Lower Left*, and *B*).

Sections of brain tumors harvested 3 h (Fig. 4*C*) and 6 h after i.v. injection of P/LLL/AON/Hu/Ms with labeled AON and PMLA were analyzed by confocal microscopy. As shown in Fig. 4*C*, positive signals for both Alexa Fluor 680 (PMLA label) and Lissamine (AON label) were seen mainly in tumor cells and also in tumor vessels positive for von Willebrand factor (vWF) staining. Both moieties showed noticeable codistribution in the cytoplasm of tumor cells (Fig. 4*C*, *Lower*). Normal brain regions of the same animals showed little drug accumulation (Fig. 4*C*, *Upper*), in agreement with whole brain imaging (Fig. 4*A*). The data suggest that nanoconjugate is efficiently passing through BTB and internalizing into the tumor cells.

Significant Suppression of Tumor Growth and Vascularity by P/LLL/AON/Hu/Ms Nanoconjugate. Systemic multiple treatments of mice bearing intracranial human glioma U87MG with nanoconjugate P/LLL/AON/Hu/Ms blocking laminin-411 synthesis significantly suppressed tumor growth (Fig. 5*A*). The mean tumor volume was 4 mm^3 ($P < 0.001$ vs. PBS), compared with 18 mm^3 ($P < 0.01$ vs. PBS) after P/LOEt/AON/Hu/Ms treatment and with 47 mm^3 in PBS-treated controls. Tumor size reduction by P/LLL/AON/Hu/Ms with pH-dependent LLL escape unit was highly significant, resulting in 90% smaller tumors compared with PBS-treated animals. LLL-containing nanoconjugate was also more than 2-fold more efficient in inhibiting tumor growth than the variant with LOEt. This result fully corroborated in vitro data on laminin-411 inhibition (Fig. 3*B*). On brain sections of PBS-treated animals, large invasively growing tumors were seen, whereas after P/LLL/AON/Hu/Ms treatment, tumor remnants with significant necrosis were typically found (Fig. 5*B*). Two conjugates without AON or anti-TfR mAbs were used as controls with no effect on tumor treatment compared with PBS, confirming that AONs against two laminin-411 chains acted as antiangiogenic inhibitors to slow down tumor growth. Morphometric analysis of vascularity on tumor sections revealed largely similar vessel numbers in all treatment groups. However, P/LOEt/AON/Hu/Ms and P/LLL/AON/Hu/Ms treatments usually resulted in smaller vessels than in the PBS group, with a significant reduction of vessel area ($P < 0.001$ vs. PBS for both nanoconjugates). The vessel area decrease was more pronounced for P/LLL/AON/Hu/Ms (over 50% less than for PBS group) than for P/LOEt/AON/Hu/Ms ($P < 0.05$) (Fig. 5*C*). On immunostained tumor sections, laminin α4 and β1 chain signal was typically strong in the tumor blood vessel basement membranes in the PBS group, and many large vessels with irregular shape were seen (Fig. 5*D*). After P/LOEt/AON/Hu/Ms, and especially P/LLL/AON/Hu/Ms treatment, staining intensity was noticeably diminished for both laminin chains (Fig. 5*D*), and vessels became more similar in size to those in normal brains.

Discussion

A number of approaches for targeted drug delivery have emerged, including encapsulation of cargo into micelles, nanospheres, nanocapsules, and nanotubes (29). Nanoconjugates as covalent delivery devices received wide interest after the introduction of natural and synthetic polymers and dendrimers (2, 17, 22, 30–34). The problems still shared by most delivery platforms include toxicity, immunogenicity, the absence of real biodegradability (i.e., lack of degradation to CO_2 and H_2O), and the target cell's cytoplasm drug delivery. Current drug design strategies are mostly focused on bioavailability and tissue targeting but rarely address drug delivery to specific intracellular compartments (35).

By introducing nanoconjugates, which use PMLA of the slime mold *Physarum polycephalum* as a platform, we have overcome most of the major drawbacks (9, 24, 30, 35–37). PMLA-based

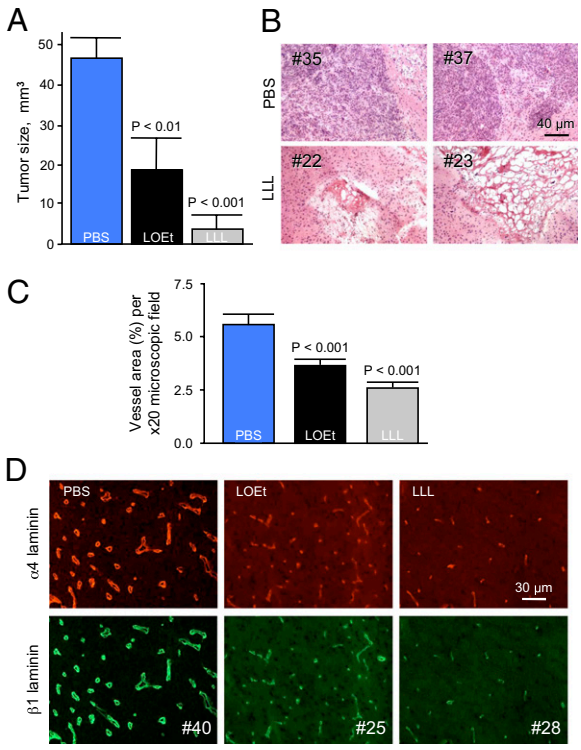

Fig. 5. Efficacy of different pH-dependent or -independent endosomal escape units in inhibiting brain tumor growth, vascularity, and target protein expression. P/LLL/AON/Hu/Ms and P/LOEt/AON/Hu/Ms were injected i.v. at 5 mg/kg morpholino AONs to laminin-411 α4 and β1 chains. (*A*) Tumor size quantitation after treatment with P/LLL/AON/Hu/Ms or P/LOEt/AON/Hu/Ms. Both nanoconjugates significantly decreased tumor volume. However, volume decrease for P/LLL/AON/Hu/Ms (LLL) with pH-dependent unit was significantly greater than for P/LOEt/AON/Hu/Ms (LOEt) with pH-independent unit. (*B*) H&E-stained sections of tumors treated by either PBS or the lead drug P/LLL/AON/Hu/Ms (LLL). Two different animals represent each group. In PBS-injected mice (#35 and #37), invasively growing intact tumors are seen. In the LLL-treated animals (#22 and #23), massive necrosis is visible with some tumor remnants. (*C*) Morphometric analysis of microvessel area after various treatments. Both P/LOEt/AON/Hu/Ms (LOEt) and P/LLL/AON/Hu/Ms (LLL) significantly reduced vessel area (most pronounced in the latter group), compared with PBS. In the LLL group, the reduction was significantly greater than in the LOEt group ($P < 0.05$). Data are from 25 nonoverlapping fields of view per group (field area = 0.245 μm^2) using 20× objective (five per tumor, five tumors per group). Percentage of area occupied by vessels (revealed by laminin β1 chain immunostaining) to total field area is shown. (*D*) Immunostaining of tumor sections for laminin α4 and β1 chains upon nanoconjugate treatment. In the PBS group, vessels stained brightly for both chains and many large vessels with irregular shapes were seen. Upon treatment with P/LOEt/AON/Hu/Ms (LOEt) and especially P/LLL/AON/Hu/Ms (LLL), tumor staining intensity for both chains was diminished and vessels became smaller, more similar to normal brain vessels. Representative pictures for each group are shown. For each antigen, exposure times were the same among groups.

nanoconjugates can deliver AON drugs into cells in vitro (38) or upon injection into the tumor mass (30), but their systemic administration with tumor cell-cytoplasm delivery (35) was not explored previously. Gliomas are highly invasive tumors, and only systemic treatment could be really beneficial to treat this very aggressive type of brain cancer. The problems now appear to be largely solved by introducing a pH-dependent endosomal escape unit, the tripeptide LLL that facilitates specific cytoplasm delivery from late endosomes (Fig. 1*A* and Fig. S1).

LLL conjugation with 40% pendant PMLA carboxyls resulted in a considerable pH-dependent membrane leakage both in liposomes and cells. Out of many hydrophobically modified PMLA structures tested, P/LLL was uniquely found to specifically respond to pH in liposome leakage assay. Its pH-dependent membranolytic activity with an operational pK_a 5.5 matched acidification during maturation from early to late endosomes. In contrast to the previously used membranolytic unit LOEt, the LLL unit was nontoxic at all concentrations tested (Fig. 3). We explain the LOEt cytotoxicity by its lipophilicity at physiological pH ~7 that renders it sticky and destructive to cell membranes. In contrast, LLL is not sticky at this pH due to its terminal negative charge. Importantly, the absence of stickiness to membranes may also prevent lipophilic units from binding to cell membranes in vascular cells in vivo and to hydrophobic sites of proteins such as opsonins of the reticuloendothelial system (39), thus contributing to reduction of nonspecific effects on nontarget cells.

The pH-restricted membranolysis is important for an optimal target bioavailability of systemically administered drugs. This indeed was borne out for LLL- versus LOEt-containing nanoconjugate, seen as an increased inhibition of target laminin-411 production in vitro and in vivo (Figs. 3*B* and 5*D*), higher tumor accumulation (Fig. 4), and significantly increased antitumor efficacy possibly related to reduced production of laminin-411 chains and decreased angiogenesis (Fig. 5 *C* and *D*). The dual effect of reducing cytotoxicity and increasing bioavailability to the target cells as opposed to nontarget ones underlies the greatly improved efficiency of the nanoconjugate–LLL drug delivery system. To our knowledge, the application of a pH-dependent endosome escape unit in drugs administered i.v. for brain cancer treatment has not been reported thus far.

A major problem in glioma treatment is the inefficiency of systemic water-soluble delivery systems due to BTB, which was bypassed in our nanoconjugate by tandem conjugated anti-mouse and anti-human TfR mAbs. The nanoconjugate actively passed the endothelial barrier by a well-established mechanism of transcytosis (11, 40, 41). BTB permeation was additionally facilitated by EPR effect (42). However, alone, transcytosis- and EPR-mediated permeation were not efficient for nanoconjugate accumulation in the tumor (Fig. 4*A*, *Upper Left* and *Center*). The second (anti-human) mAb allowed the polymer to specifically bind to and get internalized by implanted human tumor cells (Fig. 4). The move of nanoconjugate from interstitial space into the tumor cell cytoplasm mediated by anti-human TfR is important for successful accumulation and delivery. For future treatment of brain tumors in humans, two anti-species mAbs are unnecessary. However, the technical possibility of attaching two mAbs to the polymer was important in our study with xenogeneic tumors to prove the mechanisms of transcytosis through mouse endothelium and active receptor-mediated human tumor cell-specific targeting.

After endosome internalization, the LLL escape unit is activated during maturation to late endosomes concomitantly with acidification. The delivery platform and AONs remain conjugated until the disulfide linkage preserved during transcytosis (40) is cleaved by reduction with cytoplasmic glutathione. After their cytoplasmic release, free AONs can block synthesis of α4 and β1 chains of laminin-411, a basement membrane protein up-regulated in tumor neovasculature (5, 6, 30, 38). This systemic anti-angiogenic approach resulted in a specific and significant inhibition of brain tumor vascularity and growth (Fig. 5).

Safety and efficiency are two primary concerns for designing systems for AON delivery. Our PMLA-based nanoconjugates meet both criteria and offer promising strategies in systemic drug delivery to treat brain tumors and other brain degenerative conditions such as multiple sclerosis and Alzheimer's disease. Because of their biodegradability, and lack of toxicity and immunogenicity, variants of PMLA-based delivery systems can be designed for a wide array of safe and efficient applications.

Materials and Methods

Cell Viability and Cell Death Assays. Cell viability was quantified using CellTiter 96 AQueous One Solution Cell Proliferation Assay kit (Promega) and a Spec-

traMax Plus 384 ELISA reader (Molecular Devices) at A_{490} for human gliomas U87MG and TG98 and breast cancer cell line MDA MB-231.

Apoptosis and/or necrosis induced by incubation of human glioblastoma U87MG cells with 250 μg/mL of P/LLL and P/LOEt were assayed as follows. Cells were seeded in 96-well plates (1×10^4 cells per well) for 24 h and then treated with P/LLL and P/LOEt in culture medium (Eagle's MEM with 10% FBS) for 24 h. Apoptosis was measured by flow cytometry using FITC Annexin V apoptosis detection kit (BD Pharmingen). Cells stained with FITC Annexin V represented apoptosis, and those positive for PI were presumed to be necrotic (BD FACScan Flow Cytometer).

Tumor Treatment in Vivo. Animals were treated according to the approved Cedars-Sinai Medical Center Institutional Animal Care and Use Committee protocols. Athymic mice (CrTac:NCr-Foxn1nu homozygous) were from Taconic. Human U87MG glioblastoma cells were stereotactically implanted at 5×10^4 into the right basal ganglia field of mice (n = 8 per group) as reported (24). Nanoconjugate treatment began after day 8 by i.v. injecting nanoconjugates at doses of 5 mg/kg AONs on every third day, amounting to eight injections in total. Mice were killed on day 48 after cell inoculation, and tumor volumes were measured using histological sections (43) stained with H&E.

Imaging Analysis in Vivo. On days 20–30 after tumor implantation, 100 μL solution of 3 μM Alexa Fluor 680-labeled nanoconjugates was injected i.v. Mice were euthanized after 24 h. Following blood vessel clearance by intraarterial PBS perfusion for 20 min, brains were removed for fluorescence imaging by Xenogen 200 Living Image System 2.50 (Caliper Life Sciences). Light intensities emitted from equally sized surface areas of tumor and nontumor references were measured. In some cases, tumor/reference intensity ratios were calculated. The reference area was in the brain but distant from the tumor. Nanoconjugates without fluorescent Alexa Fluor 680 (background) gave negative results. Injected free dye was rapidly cleared and did not result in imaging signal (9).

Statistical Analysis. Statistical analysis was done using Prism4 statistical program (GraphPad). Data in several groups were compared using ANOVA. Data points represent mean ± SD of triplicates; in some cases in Fig. 2, SD bars were too small to be shown. In some experiments, data are expressed as mean ± SEM. $P < 0.05$ was considered significant.

Materials, Syntheses, Liposome Leakage Assay, Cell and Tissue Section Immunostaining, Colocalization Studies, and Western Blot Analysis. Materials, syntheses, liposome leakage assay, cell and tissue section immunostaining, colocalization studies, and Western blot analysis are presented in detail in *SI Materials and Methods*.

ACKNOWLEDGMENTS. We thank Dr. J. Young from the Department of Comparative Medicine, Cedars-Sinai Medical Center, for help and advice with animals. This work was supported by National Institutes of Health Grants CA123495 (to J.Y.L.) and EY13431 (to A.V.L.), Winnick Family Foundation, and M01 RR00425 (to A.V.L. and J.Y.L.), and a grant from the Department of Neurosurgery, Cedars-Sinai Medical Center.

1. Brandsma D, van den Bent MJ (2007) Molecular targeted therapies and chemotherapy in malignant gliomas. *Curr Opin Oncol* 19:598–605.
2. Folkman J (2007) Angiogenesis: An organizing principle for drug discovery? *Nat Rev Drug Discov* 6:273–286.
3. Benny O, et al. (2008) An orally delivered small-molecule formulation with antiangiogenic and anticancer activity. *Nat Biotechnol* 26:799–807.
4. Chi AS, Norden AD, Wen PY (2009) Antiangiogenic strategies for treatment of malignant gliomas. *Neurotherapeutics* 6:513–526.
5. Ljubimova JY, et al. (2001) Overexpression of alpha4 chain-containing laminins in human glial tumors identified by gene microarray analysis. *Cancer Res* 61:5601–5610.
6. Ljubimova JY, et al. (2004) Association between laminin-8 and glial tumor grade, recurrence, and patient survival. *Cancer* 101:604–612.
7. Taylor EM (2002) The impact of efflux transporters in the brain on the development of drugs for CNS disorders. *Clin Pharmacokinet* 41:81–92.
8. Cecchelli R, et al. (2007) Modelling of the blood-brain barrier in drug discovery and development. *Nat Rev Drug Discov* 6:650–661.
9. Lee BS, et al. (2006) Polycefin, a new prototype of a multifunctional nanoconjugate based on poly(β-L-malic acid) for drug delivery. *Bioconjug Chem* 17:317–326.
10. Coloma MJ, et al. (2000) Transport across the primate blood-brain barrier of a genetically engineered chimeric monoclonal antibody to the human insulin receptor. *Pharm Res* 17:266–274.
11. Zhang Y, Pardridge WM (2005) Delivery of β-galactosidase to mouse brain via the blood-brain barrier transferrin receptor. *J Pharmacol Exp Ther* 313:1075–1081.
12. Pardridge WM (2003) Blood-brain barrier drug targeting: The future of brain drug development. *Mol Interv* 3:90–105.
13. Ningaraj NS, Rao MK, Black KL (2003) Adenosine 5′-triphosphate-sensitive potassium channel-mediated blood-brain tumor barrier permeability increase in a rat brain tumor model. *Cancer Res* 63:8899–8911.
14. Duncan R (2006) Polymer conjugates as anticancer nanomedicines. *Nat Rev Cancer* 6: 688–701.
15. Satchi-Fainaro R, et al. (2004) Targeting angiogenesis with a conjugate of HPMA copolymer and TNP-470. *Nat Med* 10:255–261.
16. Torchilin VP (2008) Cell penetrating peptide-modified pharmaceutical nanocarriers for intracellular drug and gene delivery. *Biopolymers* 90:604–610.
17. Boussif O, et al. (1995) A versatile vector for gene and oligonucleotide transfer into cells in culture and in vivo: Polyethylenimine. *Proc Natl Acad Sci USA* 92:7297–7301.
18. Lv H, Zhang S, Wang B, Cui S, Yan J (2006) Toxicity of cationic lipids and cationic polymers in gene delivery. *J Control Release* 114:100–109.
19. Li W, Nicol F, Szoka FC, Jr (2004) GALA: A designed synthetic pH-responsive amphipathic peptide with applications in drug and gene delivery. *Adv Drug Deliv Rev* 56:967–985.
20. Plank C, Zauner W, Wagner E (1998) Application of membrane-active peptides for drug and gene delivery across cellular membranes. *Adv Drug Deliv Rev* 34:21–35.
21. Futaki S, et al. (2005) Unique features of a pH-sensitive fusogenic peptide that improves the transfection efficiency of cationic liposomes. *J Gene Med* 7:1450–1458.
22. Miyata K, Fukushima S, Nishiyama N, Yamasaki Y, Kataoka K (2007) PEG-based block catiomers possessing DNA anchoring and endosomal escaping functions to form polyplex micelles with improved stability and high transfection efficacy. *J Control Release* 122:252–260.
23. Davis ME, Chen ZG, Shin DM (2008) Nanoparticle therapeutics: An emerging treatment modality for cancer. *Nat Rev Drug Discov* 7:771–782.
24. Fujita M, et al. (2007) Brain tumor tandem targeting using a combination of monoclonal antibodies attached to biopoly(β-L-malic acid). *J Control Release* 122: 356–363.
25. Fu FN, Singh BR (1999) Calcein permeability of liposomes mediated by type A botulinum neurotoxin and its light and heavy chains. *J Protein Chem* 18:701–707.
26. Yessine MA, Leroux JC (2004) Membrane-destabilizing polyanions: Interaction with lipid bilayers and endosomal escape of biomacromolecules. *Adv Drug Deliv Rev* 56: 999–1021.
27. Chen R, Khormaee S, Eccleston ME, Slater NK (2009) The role of hydrophobic amino acid grafts in the enhancement of membrane-disruptive activity of pH-responsive pseudo-peptides. *Biomaterials* 30:1954–1961.
28. Abramoff MD, Magelhaes PJ, Ram SJ (2004) Image processing with ImageJ. *Biophotonics International* 11:36–42.
29. Haley B, Frenkel E (2008) Nanoparticles for drug delivery in cancer treatment. *Urol Oncol* 26:57–64.
30. Fujita M, et al. (2006) Inhibition of laminin-8 in vivo using a novel poly(malic acid)-based carrier reduces glioma angiogenesis. *Angiogenesis* 9:183–191.
31. Kopeček J, Kopecková P, Minko T, Lu Z (2000) HPMA copolymer-anticancer drug conjugates: Design, activity, and mechanism of action. *Eur J Pharm Biopharm* 50: 61–81.
32. Kopeček J, Kopecková P, Minko T, Lu ZR, Peterson CM (2001) Water soluble polymers in tumor targeted delivery. *J Control Release* 74:147–158.
33. Nori A, Kopecek J (2005) Intracellular targeting of polymer-bound drugs for cancer chemotherapy. *Adv Drug Deliv Rev* 57:609–636.
34. Duncan R (1992) Drug-polymer conjugates: Potential for improved chemotherapy. *Anticancer Drugs* 3:175–210.
35. Rajendran L, Knölker HJ, Simons K (2010) Subcellular targeting strategies for drug design and delivery. *Nat Rev Drug Discov* 9:29–42.
36. Ljubimova JY, et al. (2008) Poly(malic acid) nanoconjugates containing various antibodies and oligonucleotides for multitargeting drug delivery. *Nanomedicine (Lond)* 3:247–265.
37. Segal E, Satchi-Fainaro R (2009) Design and development of polymer conjugates as anti-angiogenic agents. *Adv Drug Deliv Rev* 61:1159–1176.
38. Khazenzon NM, et al. (2003) Antisense inhibition of laminin-8 expression reduces invasion of human gliomas in vitro. *Mol Cancer Ther* 2:985–994.
39. Owens DE, 3rd, Peppas NA (2006) Opsonization, biodistribution, and pharmacokinetics of polymeric nanoparticles. *Int J Pharm* 307:93–102.
40. Kang YS, Voigt K, Bickel U (2000) Stability of the disulfide bond in an avidin-biotin linked chimeric peptide during in vivo transcytosis through brain endothelial cells. *J Drug Target* 8:425–434.
41. Lu W, Tan YZ, Hu KL, Jiang XG (2005) Cationic albumin conjugated pegylated nanoparticle with its transcytosis ability and little toxicity against blood-brain barrier. *Int J Pharm* 295:247–260.
42. Maeda H, Wu J, Sawa T, Matsumura Y, Hori K (2000) Tumor vascular permeability and the EPR effect in macromolecular therapeutics: A review. *J Control Release* 65: 271–284.
43. Jensen MM, Jørgensen JT, Binderup T, Kjaer A (2008) Tumor volume in subcutaneous mouse xenografts measured by microCT is more accurate and reproducible than determined by ^{18}F-FDG-microPET or external caliper. *BMC Med Imaging* 8:16.